Int J Adv Manuf Technol (2018) 94:1849–1856
DOI 10.1007/s00170-017-0976-8

ORIGINAL ARTICLE

Bending processing and mechanism of laser forming pure aluminum metal foam

Min Zhang [1,2] · ChengJun Chen [1,2] · Yong Huang [1] · Tao Zou [2]

Received: 4 March 2017 / Accepted: 14 August 2017 / Published online: 30 August 2017
© Springer-Verlag London Ltd. 2017

Abstract Laser forming of pure aluminum closed-cell foam has been studied by means of an effective and cellular model, and the results are compared with experiments and numerical simulations. In order to reveal the forming process and bending mechanism during the process of laser forming closed-cell foam aluminum, a simulation was performed. It is the first time to study the laser forming pure aluminum closed-cell foam aluminum when compared to Al-Si closed-cell foam aluminum. It is found that the bending angle increases with increasing the laser power, and decreases with the increasing scan velocity in the experiment results. The stress/strain profile is similar to that in laser forming Al-Si foam aluminum in simulation results. It is confirmed that temperature gradient mechanism (TGM) is the dominant mechanism during the present laser forming of the closed-cell pure aluminum foam material. And the plastic compressive strain is caused by overall response of the cell wall bending and cell bucking, not by the material shortening.

✉ ChengJun Chen
503047820@qq.com

Min Zhang
63606536@qq.com

Yong Huang
hyorhot@lut.cn

Tao Zou
13818809291@126.com

[1] State Key Laboratory of Advanced Processing and Recycling of Non-ferrous Metals, Lanzhou University of Technology, Lanzhou, Gansu 730050, China

[2] School of Mechanical and Electrical Engineering, Laser Processing Research Center, Soochow University, Suzhou 215021, Jiangsu, People's Republic of China

Keywords Pure closed-cell foam · Laser forming · Effective property model · Stress/strain

1 Introduction

Aluminum foams can be generally considered as a new material category and very attractive in the recent decade and in the near future. What is more, they are excessively used because of their novel physical and mechanical properties such as their high strength to weight ratio and their excellent shock and noise absorption properties [1]. Al foams are most commonly fabricated in form of flat panels when using conventional manufacturing methods. But in the field of other applications of car bumpers or aerospace section and railway industry components, foam aluminums must be bended to a specific shape. Unfortunately, aluminum foams are typically brittle under mechanical forming and shaping; in turn, hard-to form properties limit their wider structure application, giving curvature to a flat panel as the panel bending would result in the foam's failure. Recent previous published papers [2, 3] have shown that laser forming is an efficient way for foam panel forming.

Guglielmotti et al. studied the possibility of laser forming of aluminum foam sandwich (AFS) panels by means of a diode laser [2]. The feasibility of the laser forming process for AFS panels is confirmed by the experiment results. They found that a very good formability was observed for the laser-processed panels and very high-bending angles were reached with a proper combination of the process parameters. More recently, the feasibility of open-cell Al foams has been further studied by Quadrini et al. [3]. Different average sizes of the pores (1.5 mm for small pores and 2 mm for big pores, and the corresponding pore density: 40 and 30 pores/in., respectively) of AlSi7Mg open-cell foam aluminum and the effect of the different laser bending process parameters (mainly laser

power and scan velocity) on the forming efficiency were compared with mechanical bending tests. And recently, a 3D thermo-mechanical model was built by means of Analysis Parametric Design Language (APDL) to study the mechanical and laser bending of open-cell aluminum foam [4, 5]. The abovementioned published results provide us a method to handle open-cell foam aluminum in simulation. Although a large sample is simulated, a small amount of simulation results were shown and the simulation results cannot be compared with experimental results. The whole scanning section temperature and strain/stress time history and contours were not discussed in the reference [4, 5] of simulation of open-cell foam aluminum. However, experimental results [2, 3] have demonstrated that the bending angle of open-cell aluminum foam [3] is quite different from closed-cell aluminum foam [2] under the same laser parameters (laser power 150 W, scan velocity 6 mm/s). Simulation of the whole laser forming process of closed-cell foam Al-Si was studied and demonstrated the temperature and strain/stress distribution and furthermore revealed the laser forming mechanism of closed-cell foam in the authors' former study [6, 7]. But it also shows the evident difference in bending angle for the Al-20SiC foam aluminum and Al-7%Si eutectic foam aluminum materials [6, 7]. In the former research, crack was also observed in the bottom surface of Al-7%Si foam aluminum when the bending angle is more than 30°, which will impact the further application of the foam aluminum. After a preliminary study, there are no cracks on the bottom surface of pure aluminum foam by means of the laser forming method, so in this paper it is necessary and essential to further study the variation law of laser forming pure aluminum foam and its bending mechanism.

2 Experimental procedures

The closed-cell foam aluminum samples were made from YUAN TAI DA of Sichuan province, which was manufactured with Al by a melting foaming method. Two different densities (about 0.24 and 0.54 g/cm^3) of closed-cell aluminum foam are used as target in the present study. Two different rectangular specimens were cut from Al samples with the dimension of 100 mm × 35 mm × 10 mm and 100 mm × 35 mm × 6 mm, respectively. The pore size is about 4~8 mm (see Fig.1). The laser system used for laser forming experiments consists of a continuous-wave 500 W YAG laser (Jiangsu Yawei Ckylaser Equipment, Co., Ltd., Wuxi, China) and a computerized numerical control (CNC) X-Y-Z three-dimensional platform. The wavelength of the laser is 1064 nm, and a defocused beam diameter (circle shape) of 2 mm is adopted via optical fiber and used in the present study. The samples were scanned by the movement of a CNC three-dimensional platform. Laser forming experiments were performed at 280~350 W. The specimens were scanned across

Fig. 1 Macrophotograph of cell foam aluminum before laser forming

the entire width at scanning speed of V = 1.6 mm/s and 1.8 mm/s, and a sum of 100 passes were performed on each specimen, in sets of 10 consecutive passes. After each set, the foam aluminum was left to cool in air for 5 min and the bending angle was evaluated by measuring the vertical displacement of the specimen free end in the middle width by means of a centesimal comparator. During each laser scan, there is 80 mm length, i.e., 45 mm longer than the specimen width to assure that the irradiated zone applied constant power during the forming process. During the laser forming process, a flow of protection gas (nitrogen) was provided on the irradiated zone so as to maximize the bending efficiency and to reduce oxidation at elevated temperature.

2.1 Mathematical analysis

It is hard work to simulate laser forming of foam materials due to its complex cellular geometry and special properties. One should modify the energy equation pertinent to laser forming in order to incorporate the presence of pores in the foam Al samples due to its consisting of pores. Therefore, with the assumption of effective properties resembling closed-cell foam samples, the continuum conservation equations are used in the simulations. Taking into account this method, temperature and stress fields are predicted numerically in the laser cutting foam Al [8] and in laser welding lotus-type porous magnesium in line with the experimental conditions [9]. For laser forming foam aluminum, the authors also demonstrated that it is an effective method to use effective properties and cellular model resembling closed-cell foam workpiece properties. So in this paper, an effective model is proposed for the closed-cell foam pure aluminum with the assumption of effective properties resembling aluminum foam in laser forming closed-cell foam aluminum (Fig. 2). Thermal and mechanical laser bending of closed-cell pure aluminum foam is simulated; a laser forming mechanism was investigated in the present paper.

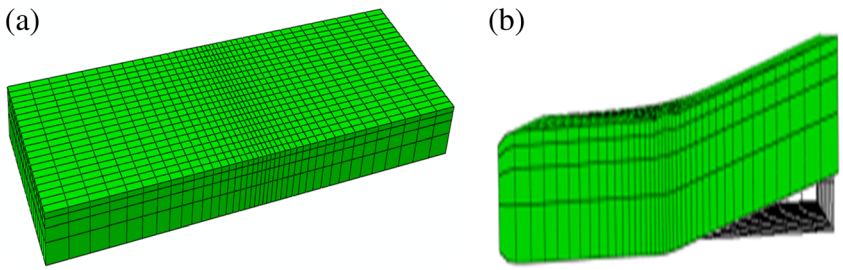

Fig. 2 Effective model profile. **a** Before bending. **b** After bending (×20)

Assumptions made for laser forming foam aluminum plate by ABAQUS during thermal analysis are listed as the following: (1) The thermal properties are isotropic; (2) the laser intensity distribution of Gaussian distribution is assumed; (3) heat conduction in the specimen, free convection, and thermal radiation in the surrounding air are considered; (4) no melting during the process of laser foaming foam aluminum is supposed; and (5) the heat due to the strain energy is neglected.

The initial temperature of the specimens is granted to be the ambient temperature 300 K. Based on the initial thermal boundary conditions and the material properties, the transient temperature distribution is solved with the heat flux over every node of the elements in ABAQUS. The solution is then substituted into the mechanical model for stress analysis.

For a coordinate system used for both thermal and mechanical models, the X-Y plane is assumed to be the laser scanning plane. In this plane, Z = 0 and X-direction are set as the laser scanning plane. And the bottom surface of specimen has positive direction, which is Z-direction.

2.2 Stress analysis

In this paper, for an effective mechanical model, three-dimensional finite element analysis is carried out incorporating ABAQUS/standard dynamic-implicit code using the crushable foam model with isotropic hardening [9]. The mechanical behavior of the metal foam is quite different from that of solid metal. Classical plastic theory cannot be used to describe their behaviors. Deshpande and Fleck [10] developed a 3D model primarily based on the experimental tests of aluminum foam, which has been built in the finite element package ABAQUS [11]. The model assumes similar behaviors in tension and compression, hence the isotropic hardening. This model has the simplest expression and has found widespread applications [9]. This stress analysis is coupled with the previous thermal analysis to import the thermal history during the laser treatment process. The crushable foam plasticity model available in ABAQUS is based on the assumption that the resulting deformation is not recoverable instantaneously and can be idealized as plastic for short duration events.

The flow potential for the isotropic hardening model is chosen as

$$G = \sqrt{q^2 + \beta^2 p^2} \tag{1}$$

$$\beta = \frac{3}{\sqrt{2}} \sqrt{\frac{1-2v_p}{1+v_p}} \tag{2}$$

Here, q is the von Mises equivalent stress and p is the mean stress.$v_p$is the plastic poisson's ratio given by

$$v_p = \frac{3-k_2}{6} \tag{3}$$

Here, k is the ratio of initial yield stress in uniaxial compression and initial yield stress in hydrostatic compression. The plastic strain is

$$\dot{\varepsilon}^{pl} = \dot{\lambda} \frac{\partial G}{\partial \sigma} \tag{4}$$

The plastic strain $\dot{\varepsilon}^{pl}$ is defined to be normal to a family of self similar, where $\dot{\lambda}$ is the non-negative plastic flow multiplier.

In the model of the FEA (finite element analysis), nonlinear analysis is used for both thermal models and mechanical models; DC3D20 is used in the thermal and mechanical models. In order to capture high gradients of temperature near the scanning path, a fine mesh is used in that region, while the coarse one is employed in remote areas. It is better for the Al foam forming process associated with the large beam diameter.

For thermal models, a user-defined subroutine is developed using FORTRAN language to define the magnitude of the heat flux, which is generated by the laser beam for top surface and porous top surface. The heat flux mainly depends on the coupled laser power, beam diameter, scanning speed, and scanning scheme. Temperature and strain rate-dependent material properties were compiled and considered in the numerical models developed for the laser forming process.

3 Results and discussion

3.1 Experimental results

Figure 3 shows the laser bending macrophotograph of pure aluminum foam after 100 passes of laser scanning. It can be

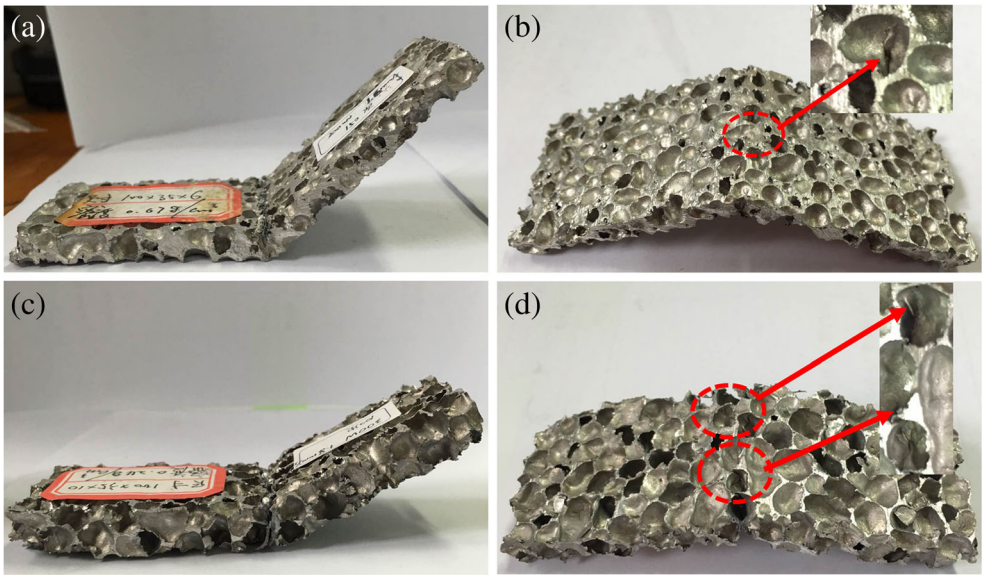

Fig. 3 Macrophotograph of cell foam aluminum after laser forming. **a** Bending specimen (6 mm). **b** The reverse side of **a**. **c** Bending specimen (10 mm). **d** The reverse side of **c**

seen that no matter how low the laser power is chosen within the processing window, localized melting of surface thin cell walls is unavoidable. It was significantly shown that the cell deformed after 100~150 passes of laser scanning; there is no

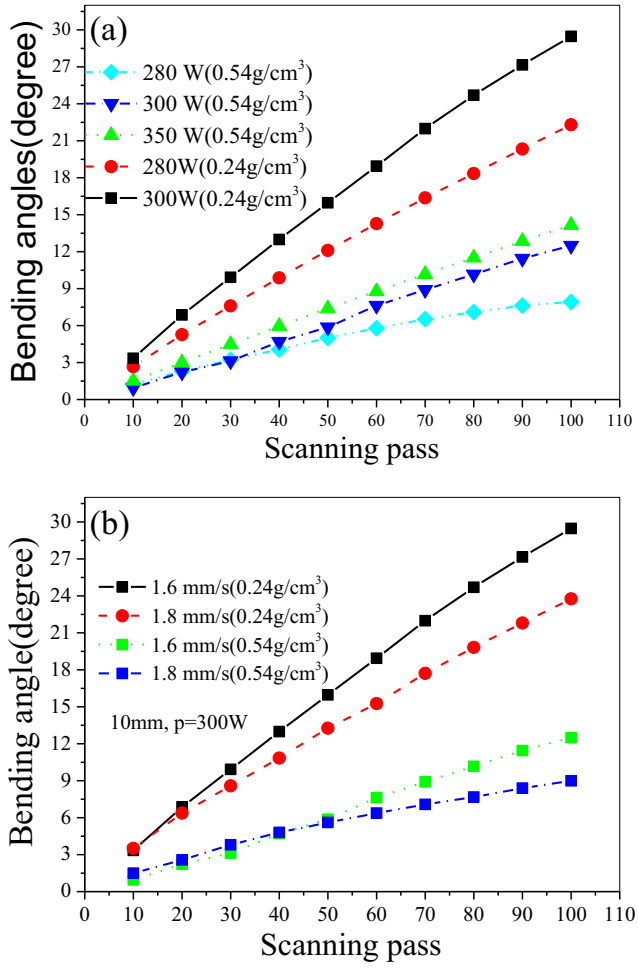

Fig. 4 Bending angle variation under different power, velocity, and density along the scanning pass. **a** Different powers and density. **b** Different velocity

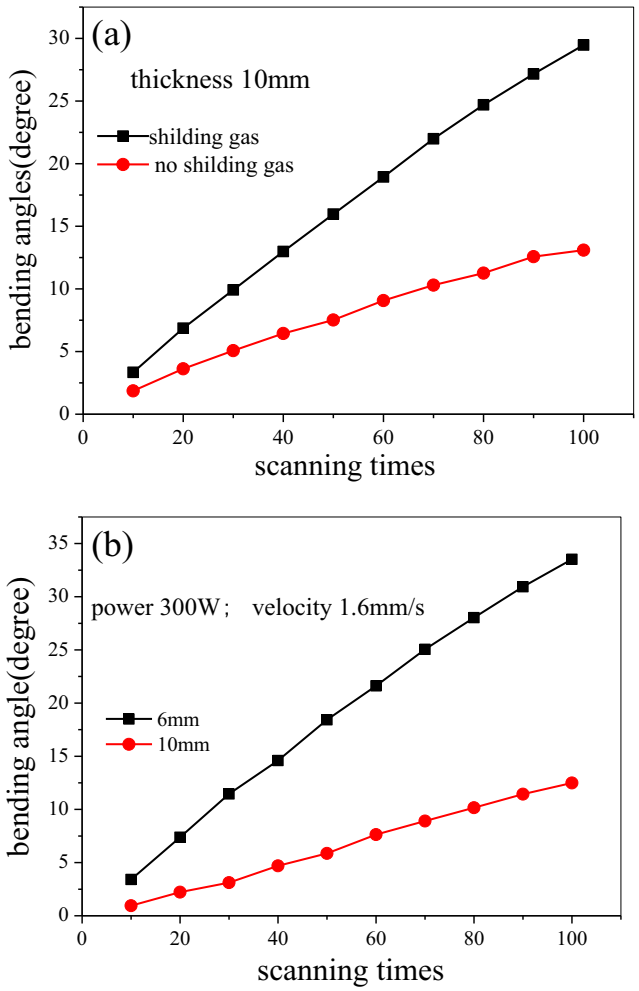

Fig. 5 Bending angle variation along the scanning pass. **a**Sheilding gas and no sheilding gas. **b** Different thickness

crack formed at the bottom surface from Fig. 3b, d. So it is very essential to further investigate the bending process of laser forming pure aluminum foam.

Figure 4 shows the bending angle of closed-cell pure aluminum foam as a function of the number of passes under different applied laser power, scan velocity values, and density. By increasing the number of passes at fixed laser power and scan velocity, the bending angle increases. As respected, the bending angle increases with increasing laser power, and decreases with increasing velocity and density. These results coincided with laser forming experiment results of Al-Si alloy closed-cell foam [2, 3].

The effect of the protective gas and thickness on the bending angle is shown in Fig. 5a, b. It is clearly found that large bending angles were obtained for shielding gas and thinner foam. In the present experiments, the bending angles in sets of 10 consecutive passes combined with different laser process parameters were compared. What is more, the effect of the scanning mode on bending angle between 10 consecutive passes and scanning 10 pass with a 5-min stop after each pass was studied. The experimental results shown in Fig. 6 illustrates that the bending angle of scanning 10 passes with a 5-min stop after each pass is higher than that 10 consecutive passes. This result coincided with the simulation results in ref. [6]; this also confirmed the accuracy of simulation of effective model in ref. [6]. Furthermore, the temperature gradient during laser scanning was affected by former laser scanning pass during 10 consecutive passes.

3.2 Numerical results and discussion

3.2.1 Analysis of thermal results

For numerical simulation of laser forming pure Al closed-cell foam, the use of an effective model to simulate the temperature history at the center of the laser interaction zone and the results is shown in Fig. 7. As expected, the temperature increases with the heating time. It can be seen that the irradiated region of the specimen is heated and the temperature is distributed almost gradient in the thickness. The temperature difference between the top and the bottom layers is much greater. So the TGM also is the main forming mechanism. Because pure aluminum foams have thermal protection and insulation function, unsymmetry of temperature field distribution also can be seen in Fig. 7; at the bottom surface, the temperature reaches its peak temperature and then later it has almost the same temperature when compared to the top surface, in which there is Δt time delay.

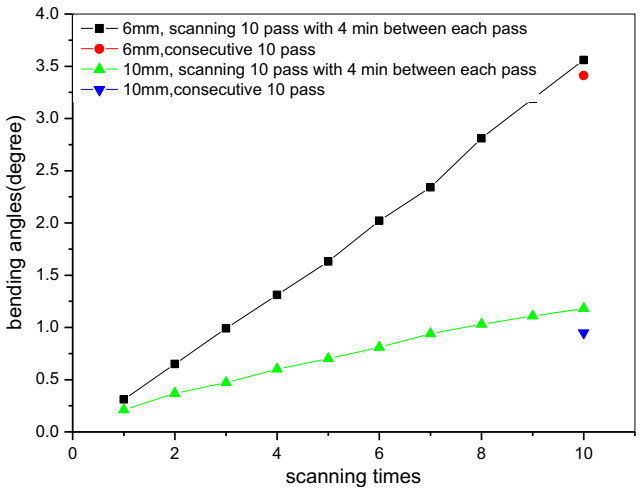

Fig. 6 Bending angle variation under consecutive and disconnected scanning

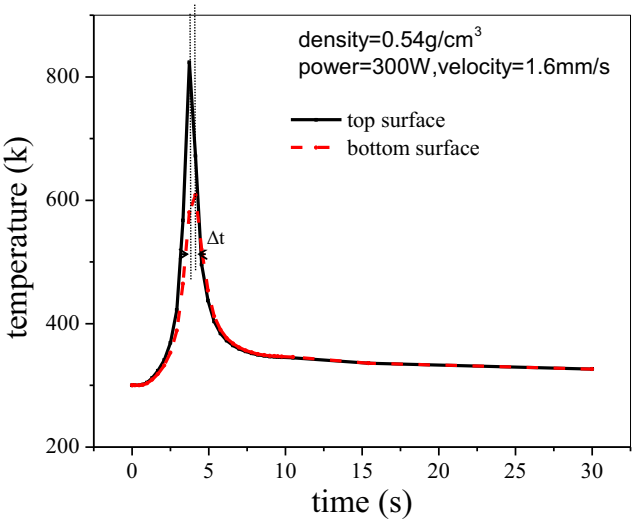

Fig. 7 Temperature history at the center of the laser interaction zone

3.2.2 Analysis of strain/stress field

A stress/strain field developed in the forming section is simulated incorporating the continuum constitutive model.

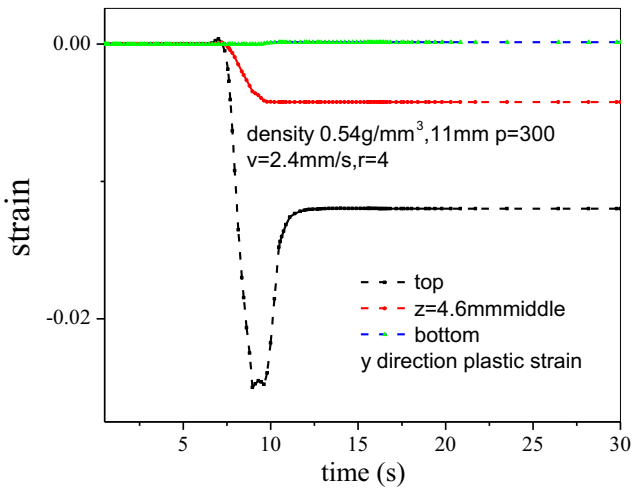

Fig. 8 Plastic strain history in the y-direction at the center of the laser interaction zone

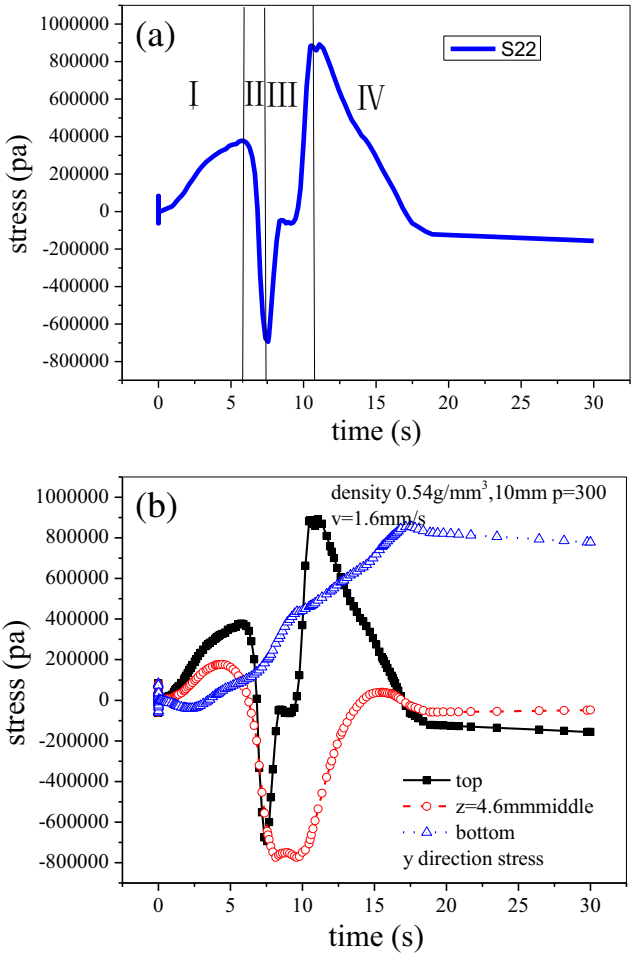

Fig. 9 Stress history in the y-direction at the center of the laser interaction zone. **a** Stress history at top surface. **b** Stress history at top/middle/bottom surface

Figure 7 demonstrates the distribution of the plastic strain after laser heating at the center of the laser interaction zone.

At the top surface, the thermal expansion converts into plastic compressive strain, which could be found in strain curves. At the beginning of laser heating, the material expands due to thermal expansion. When the heating continues, the thermal expansion begins to gradually transform into plastic strain until the cooling period begins. During the cooling process, materials not only recover to its original dimension but also shrink further, resulting in a shorter dimension. This situation is formed due to the fact that the material is plastically compressed already during heating. It is interesting to see that the compressive plastic strain recovers a little during cooling on the top surface. This is due to the fact that flow stress of the heated material is much lower than its surrounding material. At the middle surface due to thermal expansion resulting in compression strain, at the bottom surface due to the little thermal expansion and compression at the top surface, a little tension plastic strain occurs. But there are no cracks formed in the bottom surface. This is phenomenon which also confirms the fact that the plasticity of pure foam aluminum is better than Al-Si alloy foam [6].

Figure 8 shows the top/middle/bottom y-direction stress history during the laser scanning process. The stress variation is more complex when compared to strain variation. Firstly, the center point of the top surface is investigated as the target in the present study as illustrated in Fig. 8a. We can divide this process into four stages. At the beginning, the laser heats another area near this point we investigated. The thermal expansion at that point exerts tensile stress to this point. So in the first time tension, stress occurred in Fig. 8. Secondly, when the laser beam moves forward, the temperature at this point is raised (Fig. 6). The negative thermal stress increases rapidly, and the stress state changes from tensile stress to compressive stress. In the third stage, when temperature increases further, the compressive stress decreases due to the decrease in flow stress. When cooling begins, the shrinkage of the material makes the compressive stress back to tensile stress. Lastly, towards the end of laser scanning, the stress in axial direction becomes negative again. This process is quite different from that during the mechanical bending. The fact that the two processes are different is that the temperature at the end of scanning is higher than that at the beginning during laser forming foam pure aluminum. Higher temperature produces more shrinkage of material. As a result, at the top surface the material in the center of the laser scanning trace becomes compression (Fig. 8a). In the middle surface, the temperature change is smaller than that at the top surface, so the final compressive stress is lower than that at the point of top surface (Fig. 8b).

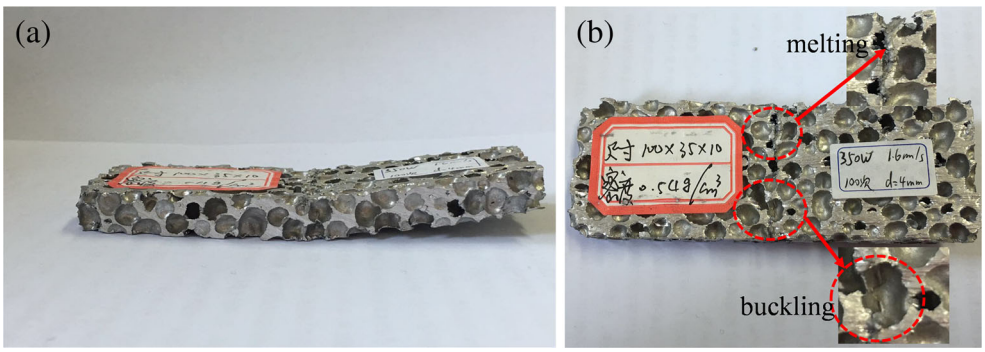

Fig. 10 The appearance of bending specimen and the bucking characteristic. **a** Bending specimen. **b** Buckling cell

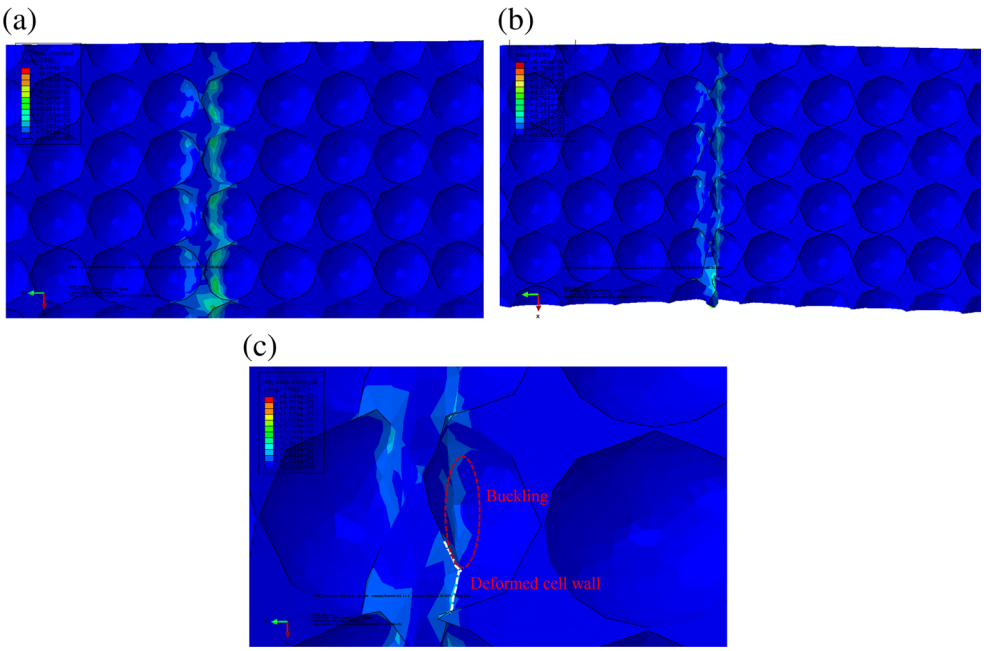

Fig. 11 Simulation results about **a** plastic strain distribution of maximum principal stress; **b** ×20 of **a**; **c** plastic strain distribution of buckling and deformed cell wall

And for the point in the bottom surface, the stress variation (Fig. 8b) is very different from the point at the top surface. Due to the fact that there exist very small changes of temperature, its stress change was mainly effected by the material properties around it. Due to the tension at the top surface at the first time, compressive stress occurred at the bottom surface as illustrated in Fig. 8. Then, because of the generation of compressive stress at the top surface, compressive stress quickly converted into tension stress at the bottom surface. The increased temperature cannot lead to the shrinkage of material because of the small increasing temperature. So as demonstrated in Fig. 8, the final stress state at the bottom surface is tension stress (Fig. 9).

From effective modeling and simulation results, the overall aluminum foam forming behavior of pure aluminum foam during the laser scanning process can be clearly seen. This is due to the fact that foam materials are quite different from solid materials and it is a non-traditional materials with a lots of pores. And the cell faces behave as weak shell-like structures at a nominal compressive strain. The effect of laser forming on the stress-strain distribution of a single pore is different from the whole foam; this phenomenon can be seen clearly in Fig. 10, which illustrates the deformation of the cell wall after laser scanning. Also, it can be observed that, the thicker the cell edge or the thinner the cell face, the more unavoidable localized melting of the thin cell occurred, as shown in Fig. 10b. In another way, the cell wall may be bended and buckled when the thickness of the cell edge or cell wall is larger enough, as shown in Fig. 10b. It is can be found that the cellular model was able to replace a similar foam geometry of real foam. This model is highly responsive to cell wall changes in simulation processing conditions. In Fig. 11, it can be seen that the bending and buckling of the cell wall agree well with the experimental results as shown in Fig. 10.

3.2.3 Displacement

Figure 12 demonstrates the Z-direction displacement along the scanning path in simulation results. For laser forming metal sheet, there are angle variations along the laser scanning direction [12]. But as to laser forming foam aluminum, it can seen that there are no variations in Z direction displacement. The abovementioned interesting phenomenon can be firmly conformed that the bending angle is almost constant along the scanning direction, which can further demonstrate that the forming in a constant thickness is uniform. So, for

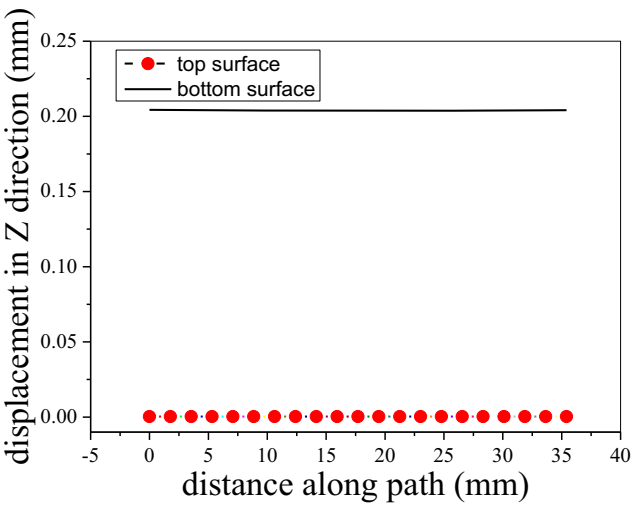

Fig. 12 The displacement in Z-direction along the scanning direction

bending foam aluminum, the laser forming process is a best choice when compared to conventional methods [13].

4 Conclusions

In this paper, the laser formability of 6- and 10–mm-thick pure aluminum closed-cell foam through experiments and numerical simulations was investigated during the present paper; the main conclusions can be drawn in the following words:

1. The current work has similar variation trends to the previous published Al-Si alloy foam under different applied laser power and scanning velocity [6].
2. After the analysis of thermal simulation results, TGM is the main laser forming mechanism for pure aluminum foam, but the present TGM is different with the traditional TGM.
3. After the analysis of the mechanical simulation results, stress at the top surface is compression stress and at the bottom surface is tension stress. Furthermore, the forming angle is uniform along the scanning path.

Acknowledgements The authors gratefully acknowledged financial support from the National Natural Science Foundation of China (51104110). It is supported by the fund of the State Key Laboratory of Advanced Processing and Recycling of Non-ferrous Metals, Lanzhou University of Technology (SKLAB02014006) and Suzhou Science and Technology Bureau with grant (No. SYG201642).

References

1. Raj RE, Daniel BSS (2008) Manufacturing challenges in obtaining tailor-made closed-cell structures in metallic foams. Int J Adv Manuf Technol 38(5–6):605–612. https://doi.org/10.1007/s00170-007-1254-y
2. Guglielmotti A, Quadrini F, Squeo EA, Tagliaferri V (2009) Laser bending of aluminum foam sandwich panels. Adv Eng Mater 11(11):902–906. https://doi.org/10.1002/adem.200900111
3. Quadrini F, Guglielmotti A, Squeo EA, Tagliaferri V (2010) Laser forming of open-cell aluminium foams. J Mater Process Technol 210(11):1517–1522. https://doi.org/10.1016/j.jmatprotec.2010.04.010
4. Loredana S, Guglielmotti A and Quadrini F, (2010) Formability of open-cell aluminium foams by laser. Paper presented at the Proceedings ASME. 2010 International Manufacturing Science and Engineering Conference MSEC2010, Erie, Pennsylvania
5. Quadrini F, Denise B, Daniele F, Loredana S, Satrsiero A (2013) Numerical simulation of laser bending of aluminum foams. Key Eng Mater 2013(554–557):1864–1871. https://doi.org/10.4028/www.scientific.net/KEM.554-557.1864
6. Zhang M, Chen CJ, Grandal G, Bian DK, Yao YL (2016) Experimental and numerical investigation of laser forming of closed-cell aluminum foam. J Manuf Sci Eng 138(2):021006–021006-8. https://doi.org/10.1115/1.4030511
7. Tizian B, Christopher B, Zhang M, Chen CJ, Lawrence YL (2016) Effect of geometrical modeling on prediction of laser-induced heat transfer in metal foam. J Manuf Sci Eng 138(12):121008–121008-11. https://doi.org/10.1115/1.4033927
8. Mukarami T, Tsumura T, Ikeda T, Nakajima H, Nakata K (2007) Ansitropic fusion profile and joint strength of lotus-type porous magnesium by laser welding. Mater Sci Eng A 456(1–2):278–285. https://doi.org/10.1016/j.msea.2006.11.162
9. Yilbas BS, Akhtar SS, Keles O (2013) Laser cutting of aluminum foam: experimental and model studies. J Manuf Sci Eng 135(5):051018–051026-9. https://doi.org/10.1115/1.4025009
10. Deshpande VS, Fleck NA (2000) Isotropic constitutive models for metallic foams. J Mech Phys Solids 48(6–7):1253–1283. https://doi.org/10.1016/S0022-5096(99)0082-4
11. ABAQUS Theory manual, version 6.9, 2009, ABAQUS Inc., Pawtucket
12. Cheng P, Fan YJ, Lawrence YL, Mika DP, Zhang WW, Graham M, Marte J, Jones M (2005) Laser forming of varying thickness plate—part1: process analysis. J Manuf Sci Eng 128(3):642–650. https://doi.org/10.1115/1.2162912
13. Tzeng SC, Ma WP (2006) A novel approach to manufacturing and experimental investigation of closed-cell Al foams. Int J Adv Manuf Technol 28(11–12):1122–1128. https://doi.org/10.1007/s00170-004-2440-9